THE ASTROPHYSICAL JOURNAL, 396:80–96, 1992 September 1

NEW CEPHEID DISTANCES TO NEARBY GALAXIES BASED ON *BVRI* CCD PHOTOMETRY. III. NGC 300

WENDY L. FREEDMAN[1]
The Observatories, Carnegie Institution of Washington, 813 Santa Barbara Street, Pasadena, CA 91101
BARRY F. MADORE[1]
NASA/IPAC Extragalactic Database, Infrared Processing and Analysis Center, Jet Propulsion Laboratory 100-22, California Institute of Technology, Pasadena, CA 91125
S. L. HAWLEY
Lawrence Livermore National Labs, Inst. Geo. and Planetary Physics, Mail Code L-413, P.O. Box 808, Livermore, CA 94550
IRWIN K. HOROWITZ AND JEREMY MOULD
Division of Physics, Mathematics and Astronomy, California Institute of Technology, MS 105-24, Pasadena, CA 91125
MAURICIO NAVARRETE
Cerro Tololo Inter-american Observatory, National Optical Astronomical Observatories, Casilla 603, La Serena, Chile 1353
AND
SHAUNA SALLMEN
Department of Astronomy, University of California, Berkeley, CA 94720
Received 1991 November 27; accepted 1992 March 6;

ABSTRACT

A true distance modulus of $(m - M)_0 = 26.66 \pm 0.10$ mag (corresponding to 2.1 ± 0.1 Mpc) has been determined for the Sculptor Group spiral galaxy NGC 300. New CCD data have been obtained for a sample of known Cepheids in this galaxy from which apparent distance moduli at *B*, *V*, *R*, and *I* wavelengths are determined. Combining the data available at different wavelengths, and assuming a true distance modulus to the LMC of 18.5 mag, a true distance modulus is obtained for NGC 300, corrected for the effects of interstellar reddening. The availability of a new distance to NGC 300 brings to five the total number of galaxies with new CCD photometry of Cepheids, useful for calibration of the Hubble constant.

Subject headings: Cepheids — galaxies: distances and redshifts — galaxies: individual (NGC 300) — Local Group — techniques: photometric

1. INTRODUCTION

For the last 8 years or so we have been undertaking to establish a consistent set of ground-based Cepheid distances to the nearest resolved late-type galaxies. The primary motivation has been to increase the number of galaxies that can be used to set the zero-point and dispersion of secondary distance indicators such as the *infrared Tully-Fisher relation* and thereby provide an accurate calibration of the Hubble constant. A further motivation has been to provide a consistent set of distances in order to study the intrinsic properties of the stellar populations in these systems. With only four galaxies (M31, M33, M81, and NGC 2403) so far studied in this way, the systematics of the zero point of the secondary distance indicators remain uncertain. A larger sample of independently distance-calibrated spiral galaxies is still required to determine an accurate zero point for the extragalactic distance scale. In this paper, a new Cepheid distance is obtained to the Sculptor Group galaxy NGC 300, bringing our total number of calibrating galaxies for the infrared Tully-Fisher relation to five.

This paper is the third in a series on the distances to nearby galaxies. The first two papers presented new CCD photometry of known Cepheids and derived distances based on those observations for IC 1613 (Freedman 1988a) and M33 (Freedman, Wilson, & Madore 1991). An ancillary paper (Freedman & Madore 1988) discussed preliminary results for the two more distant galaxies M81 and NGC 2403. In the present study, multiwavelength CCD photometry is given for 16 Cepheids in the southern-hemisphere galaxy NGC 300. A distance modulus corrected for reddening is derived. Application of this distance to the calibration of the Tully-Fisher relation has been discussed by Freedman (1990). In a future paper, photometry for the resolved stellar population will be discussed. The next paper planned in this series will give Cepheid photometry and a new distance to the Local Group spiral galaxy M31.

2. CCD PHOTOMETRY

CCD observations of Cepheids in NGC 300 were obtained at the Cerro Tololo 4 m telescope over the time interval 1985 September to 1988 November. From the second through the fourth year of the program, data were obtained in the service-observing mode offered at CTIO under the guidance of Mauricio Navarrete. For most of the runs, we used an RCA chip, having a scale of 0.″6 pixel^{-1} at the prime focus. In 1988, this chip at the 4 m was decomissioned, and a different RCA chip was substituted from one of the other CTIO telescopes. On one night (1988 November 2/3), data were taken with a TI chip. The exposure times were generally 400 s in *B*, and 300 s in *V*, *R*, and *I*. The frames were bias subtracted, flat-fielded, and defringed using standard data reduction packages available at Cerro Tololo.

At the prime focus of the CTIO 4 m, the field size of the RCA chip is $\sim 5' \times 3'$. Twelve fields in NGC 300 were observed,

[1] Visiting Astronomer, Cerro Tololo National Observatory, National Optical Astronomy Observatories, operated by the Association of Universities for Research in Astronomy, Inc., under contract with the National Science Foundation.

TABLE 1

OBSERVATIONS OF INDIVIDUAL CEPHEIDS IN NGC 300

Filter	(2,440,000+)	Magnitude	Error
	V2, $P = 17^d.84$		
B.....	6329.774	22.62	0.05
	6743.717	21.95	0.05
	7081.616	22.40	0.08
	7090.750	22.33	0.05
	7119.776	21.35	0.05
	7123.573	21.97	0.04
	7447.785	22.39	0.04
	7472.799	22.55	0.04
V.....	6329.804	21.94	0.05
	6743.709	21.56	0.04
	7070.600	21.75	0.27
	7081.622	21.81	0.07
	7090.755	21.60	0.04
	7119.771	20.99	0.03
	7123.580	21.39	0.04
	7441.834	21.14	0.02
	7447.780	21.66	0.04
	7472.806	21.89	0.05
R.....	6743.729	21.25	0.04
	7070.605	21.11	0.17
	7081.626	21.45	0.06
	7090.760	21.25	0.03
	7119.761	20.78	0.03
	7123.587	21.10	0.03
	7441.829	20.87	0.02
I.....	6329.792	21.23	0.11
	6743.735	20.95	0.10
	7070.608	20.61	0.14
	7081.630	20.99	0.16
	7090.765	20.87	0.06
	7119.753	20.60	0.06
	7123.591	20.71	0.08
	7441.822	20.58	0.04
	V3, $P = 56^d.61$		
B.....	6329.774	20.82	0.02
	6331.806	20.89	0.02
	6699.708	21.77	0.03
	6743.717	21.44	0.03
	7063.613	20.86	0.06
	7070.594	20.89	0.07
	7081.616	21.40	0.04
	7090.750	21.83	0.03
	7123.573	20.88	0.02
	7447.785	20.78	0.01
	7468.646	20.85	0.06
	7472.799	21.18	0.02
	7123.669	20.85	0.02
	7419.875	21.29	0.02
V.....	6329.804	20.16	0.03
	6331.596	20.18	0.01
	6699.721	20.80	0.02
	6743.709	20.49	0.02
	7063.620	20.28	0.18
	7070.600	20.27	0.06
	7081.622	20.48	0.02
	7090.755	20.83	0.02
	7123.580	20.19	0.02
	7441.834	20.63	0.01
	7447.780	20.26	0.01
	7468.642	20.12	0.02
	7472.806	20.38	0.02
	7123.676	20.16	0.01
	7419.881	20.40	0.01
R.....	6699.729	20.35	0.02
	6743.729	20.03	0.03
	7063.625	19.83	0.04
	7070.605	19.79	0.05
	7081.626	19.97	0.02
	7090.760	20.31	0.02
	7123.587	19.83	0.02
	7441.829	20.22	0.01
	7468.629	19.75	0.01
	7123.681	19.78	0.01
I.....	6329.7917	19.46	0.05
	6699.7368	19.85	0.04
	6743.7354	19.62	0.03
	7070.6083	19.51	0.06
	7081.6306	19.56	0.06
	7090.7646	19.82	0.03
	7123.5910	19.47	0.03
	7441.8222	19.78	0.02
	7468.6333	19.39	0.03
	7123.6854	19.35	0.03
	V9, $P = 18^d.24$		
B.....	6699.672	21.83	0.08
	6744.728	22.25	0.12
	7090.841	22.25	0.09
	7120.680	21.50	0.06
	7441.852	22.25	0.05
	7468.655	21.61	0.02
V.....	6699.662	21.08	0.07
	6744.734	21.79	0.12
	7090.835	21.59	0.07
	7120.675	21.08	0.06
	7441.844	21.64	0.05
	7468.663	21.17	0.06
R.....	669.650	20.80	0.09
	7090.821	21.09	0.05
	7120.670	20.69	0.04
	7468.671	20.83	0.03
I.....	6699.635	20.60	0.12
	7090.815	20.92	0.08
	7120.666	20.54	0.07
	7468.677	20.42	0.08
	V10, $P = 25^d.01$		
B.....	6329.728	22.60	0.09
	6406.705	22.65	0.09
	7090.792	21.55	0.03
	7120.639	21.70	0.04
	7123.630	22.04	0.05
	7419.827	21.56	0.05
	7468.722	21.48	0.04
	7472.722	21.88	0.04
V.....	6329.747	21.61	0.06
	6406.701	21.58	0.06
	7090.978	20.95	0.04
	7120.646	20.99	0.04
	7123.616	21.16	0.04
	7419.823	21.08	0.02
	7447.837	21.16	0.04
	7468.731	20.96	0.03
	7472.500	21.18	0.03
R.....	6329.715	21.05	0.07
	6406.711	21.15	0.07
	7090.803	20.69	0.04
	7120.651	20.63	0.05
	7123.621	20.79	0.04
	7447.831	20.81	0.03
	7472.710	20.79	0.03
I.....	6329.703	20.73	0.08
	6406.715	20.78	0.12
	7090.807	20.51	0.06
	7120.656	20.41	0.06
	7123.625	20.50	0.08
	7447.826	20.40	0.03
	7472.704	20.37	0.06

TABLE 1—*Continued*

Filter	(2,440,000+)	Magnitude	Error
	V12, $P = 89^d.40$		
B.....	6329.728	20.58	0.03
	6406.705	21.12	0.03
	7090.792	20.99	0.02
	7120.639	21.09	0.03
	7123.630	20.94	0.03
	7419.827	20.50	0.04
	7468.722	21.18	0.03
	7472.722	21.18	0.03
V.....	6329.747	19.50	0.04
	6406.701	19.93	0.04
	7081.765	19.56	0.04
	7090.798	19.71	0.03
	7120.646	19.87	0.04
	7123.616	19.81	0.04
	7419.823	19.63	0.01
	7447.837	19.80	0.02
	7468.731	20.05	0.02
	7472.500	20.06	0.02
R.....	6329.715	19.11	0.05
	6406.711	19.38	0.06
	7081.772	18.90	0.06
	7090.803	19.16	0.03
	7120.651	19.30	0.05
	7123.621	19.26	0.04
	7447.831	19.26	0.03
	7472.710	19.42	0.02
I.....	6329.703	18.76	0.05
	6406.715	19.02	0.06
	7081.776	18.22	0.12
	7090.807	18.72	0.03
	7120.656	18.95	0.04
	7123.625	18.83	0.04
	7447.826	18.74	0.01
	7472.704	18.90	0.05
	V20, $P = 18^d.01$		
B.....	6332.707	21.71	0.09
	7070.655	21.64	0.08
	7090.784	21.98	0.08
	7120.602	22.41	0.09
	7419.810	22.50	0.06
	7447.797	21.27	0.03
	7472.673	22.45	0.06
V.....	6332.728	21.23	0.05
	7070.662	21.09	0.08
	7081.653	21.81	0.11
	7090.780	21.29	0.04
	7120.609	21.78	0.05
	7123.609	20.93	0.07
	7419.817	21.80	0.05
	7447.805	20.90	0.03
	7472.681	21.59	0.04
R.....	6332.745	20.83	0.04
	7070.667	20.84	0.06
	7081.649	21.47	0.08
	7090.776	20.92	0.03
	7120.615	21.30	0.04
	7123.604	20.65	0.04
	7447.813	20.63	0.03
	7472.688	21.16	0.06
I.....	6332.760	20.52	0.07
	7070.671	20.43	0.15
	7081.645	20.84	0.15
	7090.771	20.54	0.06
	7120.619	20.78	0.08
	7123.599	20.39	0.08
	7447.818	20.42	0.04
	7472.692	20.68	0.09

Filter	(2,440,000+)	Magnitude	Error
	V21, $P = 9^d.67$		
B.....	7090.784	22.41	0.09
	7120.602	23.10	0.12
	7419.810	23.48	0.12
	7447.797	22.04	0.05
	7472.673	22.17	0.05
V.....	7070.662	22.07	020
	7090.780	21.73	0.06
	7120.609	21.92	0.06
	7123.609	22.25	0.11
	7419.817	22.40	0.09
	7447.805	21.52	0.04
	7472.681	21.57	0.05
R.....	7070.667	21.50	0.09
	7090.776	21.19	0.05
	7120.615	21.39	0.04
	7123.604	21.74	0.08
	7447.813	21.08	0.04
	7472.688	21.18	0.07
I.....	7070.671	20.84	0.23
	7090.771	20.75	0.08
	7120.619	21.00	0.12
	7123.599	21.24	0.16
	7447.818	20.72	0.05
	7472.692	20.81	0.09
	V22, $P = 20^d.64$		
B.....	6328.732	22.98	0.09
	7472.786	22.20	0.03
V.....	6328.711	22.25	0.08
	7472.781	21.46	0.04
R.....	6328.750	21.68	0.05
	7472.773	21.11	0.03
I.....	6328.765	21.56	0.13
	7472.768	20.70	0.05
	V24, $P = 126^d.04$		
B.....	6328.732	20.91	0.03
	7472.786	20.87	0.01
V.....	6328.711	19.84	0.02
	7472.781	19.86	0.01
R.....	6328.750	19.36	0.01
	7472.773	19.29	0.01
I.....	6328.765	18.90	0.01
	7472.768	18.85	0.02
	V25, $P = 16^d.19$		
V.....	7123.706	22.29	0.12
R.....	7123.701	20.94	0.14
I.....	7123.697	20.20	0.10
	V27, $P = 35^d.01$		
B.....	6330.712	21.05	0.02
	7082.692	22.17	0.06
	7090.725	22.67	0.05
	7119.726	22.33	0.06
	7124.712	22.52	0.06
	7419.837	21.43	0.01
	7468.708	22.20	0.03
	7472.735	22.59	0.05
V.....	6330.727	20.39	0.02
	6408.663	20.77	0.04
	7081.815	21.31	0.18

TABLE 1—*Continued*

Filter	(2,440,000+)	Magnitude	Error
	V27, $P = 35^d.01$		
	7082.699	21.03	0.06
	7090.732	21.44	0.04
	7119.741	21.18	0.04
	7124.719	21.40	0.04
	7419.845	20.59	0.01
	7472.743	21.49	0.04
R.....	6330.740	20.10	0.03
	6408.653	20.30	0.03
	7081.799	20.59	0.05
	7082.704	20.61	0.04
	7090.738	20.89	0.03
	7119.737	20.64	0.03
	7124.723	20.88	0.04
	7419.850	20.21	0.02
	7472.750	20.88	0.02
I.....	6330.752	19.79	0.04
	6408.658	19.87	0.04
	7081.807	20.07	0.08
	7090.742	20.48	0.05
	7119.731	20.14	0.04
	7124.727	20.47	0.08
	7419.855	19.86	0.02
	7472.754	20.52	0.05
	V29, $P = 23^d.44$		
B.....	6330.712	22.16	0.05
	6730.732	22.13	0.06
	7082.692	22.38	0.08
	7090.725	22.47	0.04
	7119.726	21.07	0.03
	7124.712	21.71	0.03
	7419.837	22.43	0.03
	7472.735	21.33	0.01
V.....	6330.727	21.24	0.03
	6408.663	21.67	0.05
	6730.729	21.34	0.04
	7082.699	21.56	0.10
	7090.732	21.70	0.04
	7119.741	20.73	0.04
	7124.719	21.04	0.03
	7419.845	21.75	0.04
	7472.743	20.85	0.02
	V29, $P = 23^d.44$		
R.....	6330.740	20.78	0.03
	6408.653	21.26	0.05
	6730.719	20.85	0.03
	7082.704	20.95	0.05
	7090.738	21.22	0.03
	7119.737	20.43	0.03
	7124.723	20.67	0.04
	7419.850	21.23	0.02
	7472.750	20.49	0.02
I.....	6330.752	20.45	0.05
	6408.658	20.64	0.09
	6730.724	20.43	0.06
	7090.742	20.67	0.07
	7119.731	20.36	0.05
	7124.727	20.16	0.07
	7419.855	20.79	0.04
	7472.754	20.23	0.04
	V33, $P = 24^d.24$		
B.....	7120.697	21.65	0.03
	7124.747	22.03	0.05
V.....	7120.704	21.08	0.03
	7124.743	21.31	0.04
R.....	7120.712	20.71	0.03
	7124.738	20.82	0.03
I.....	7120.716	20.25	0.06
	7124.733	20.56	0.08
	V32, $P = 52^d.76$		
B.....	6332.814	20.74	0.06
	7120.742	20.74	0.10
	7468.752	21.62	0.02
V.....	6332.806	20.17	0.06
	7120.737	20.23	0.11
	7468.747	20.62	0.02
R.....	6332.797	19.76	0.03
	7120.732	19.83	0.05
I.....	6332.788	19.45	0.06
	7120.727	19.55	0.08

containing a total of 16 known Cepheids from Graham (1984) and yielding a total of 256 frames over the course of this program. The Cepheids observed are listed in Table 1; their periods range from 9.6 to 126 days. The individual variables were originally identified by Graham in 2′ × 2′ finder charts. For convenience, we present here a photograph of NGC 300 taken from Sandage & Bedke (1988), [Fig. 1 (Pl. 1)] indicating the locations of our CCD fields, while in Figures 2*a*–2*j* we give reproductions of representative *V*-band CCD frames, showing the Cepheids themselves.

The CCD data were reduced using stellar photometry program DoPHOT (see Mateo & Schechter 1989). The details of the steps involved in this procedure are described in the above reference and in Freedman (1988b) and will not be repeated here. But briefly, DoPHOT constructs a point-spread function based on seven-parameter fits to the brightest stars in each field. Objects are then found and fit above a given threshold and they are then subtracted from the picture. The fit to the background is updated, another threshold is reached, new objects are found, and then *all* objects are remeasured, having their parameters updated. The process is repeated until the lowest specified threshold is reached. DoPHOT provides the difference between the PSF-fit magnitudes and an aperture magnitude for the brightest and best-fit stars on the frame. An aperture correction for each frame was adopted after averaging the values obtained for all the stars for which that quantity was calculated, and then rejecting points 2 σ away from the mean. In this way stars were rejected if their errors were large, while points included in the average were weighted by the intensities of the stars for which they were calculated. Final aperture corrections were obtained generally using from two to 10 stars on each frame, and the corrections are formally accurate to better than ± 0.03 mag.

E-region standards in E1, E2, E3, E7, E8, and E9 (Graham 1984) and SA 98 (Landolt 1983) were used to define the transformation equations for the calibration. Over the course of the 4 years during which the data were obtained for this program, *BVRI* standard star frames were taken on 20 independent photometric nights. The NGC 300 frames on each photometric night were all initially reduced independently to provide a measurement of the external accuracy of the final zero-point calibration. Magnitudes for the brightest stars generally agree

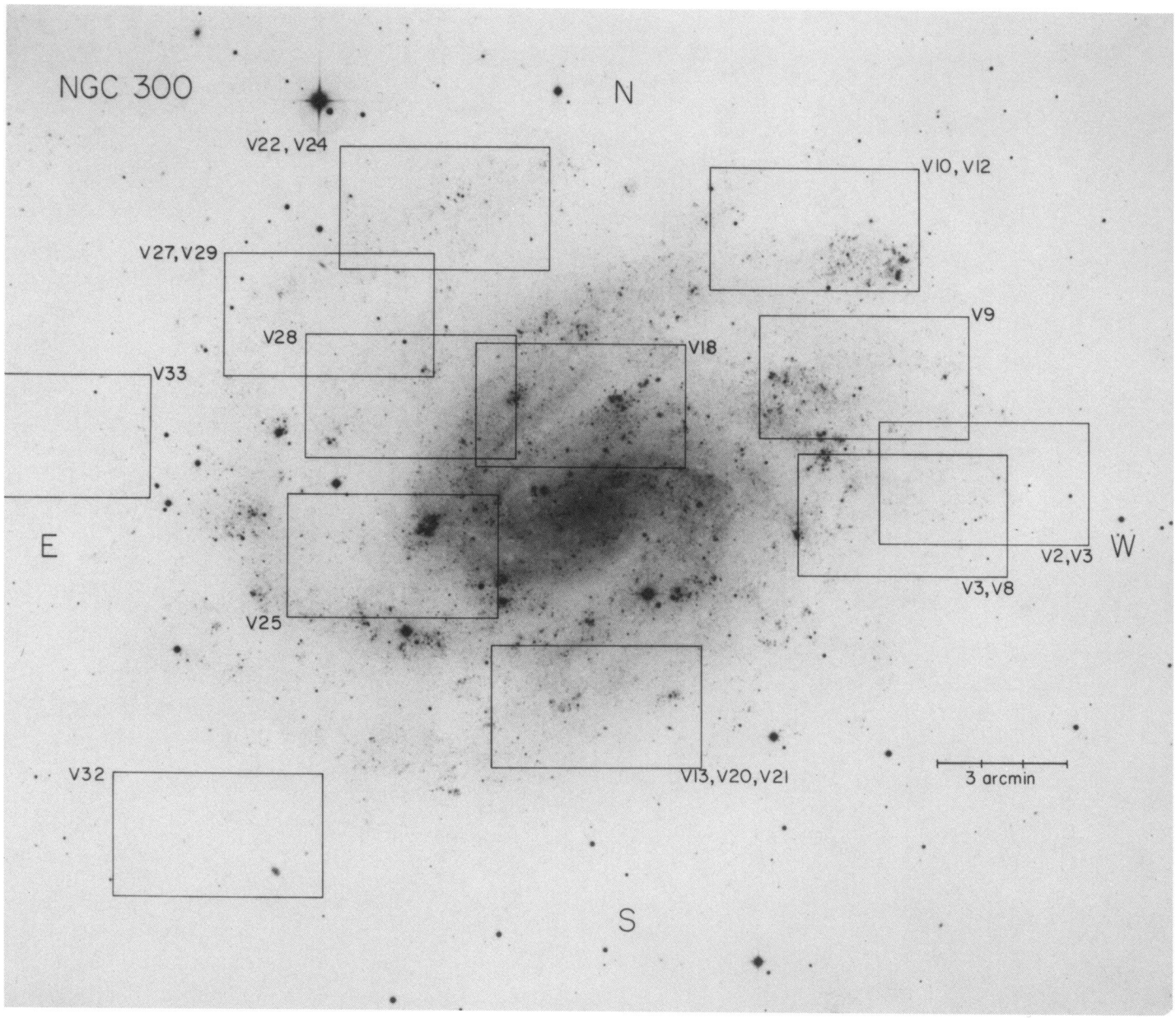

FIG. 1.—A print of NGC 300 showing the locations of the CCD frames taken at the CTIO 4 m centered on known Cepheids in that galaxy

FREEDMAN et al. (see 396, 83)

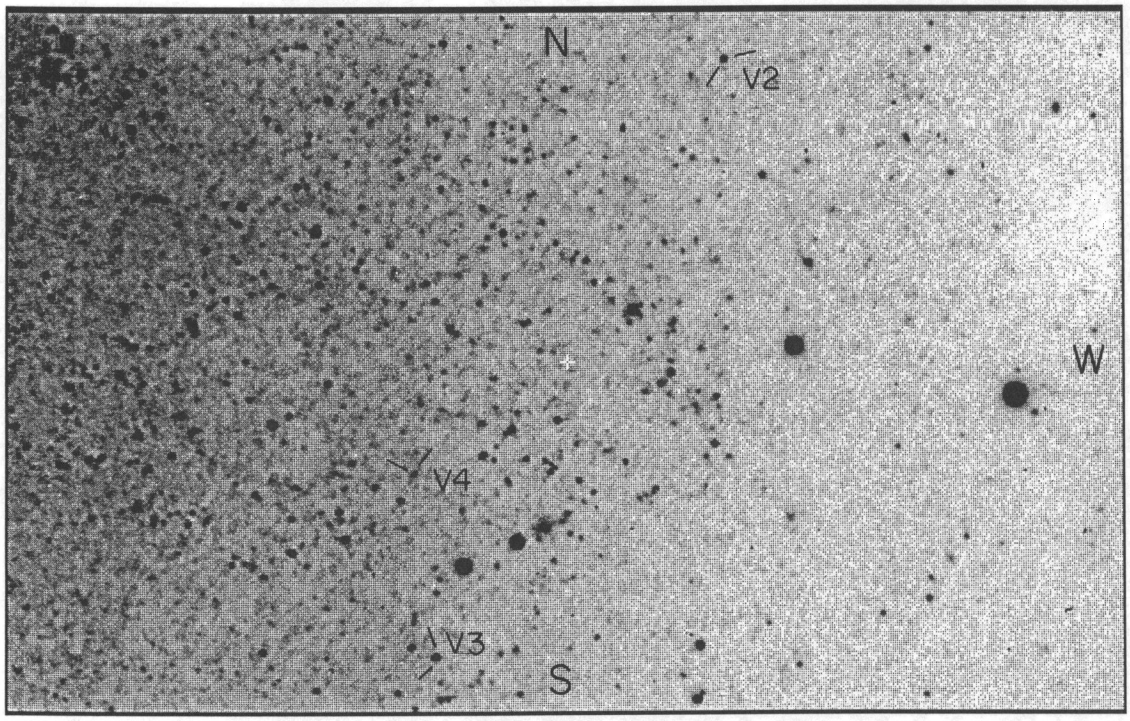

FIG. 2a

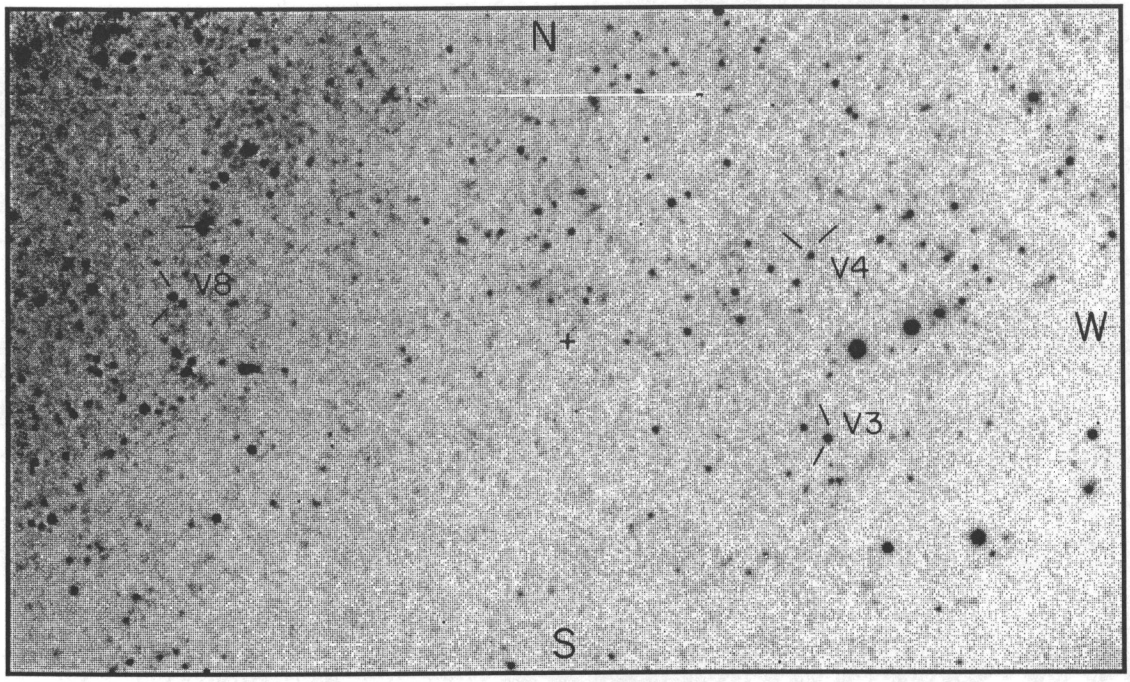

FIG. 2b

FIG. 2.—(*a–j*) Reproductions of *V*-band CCD images of the NGC 300 Cepheid fields as identified in Fig. 1. North is at the top, west is to the right. The field covered is $\sim 5' \times 3'$.

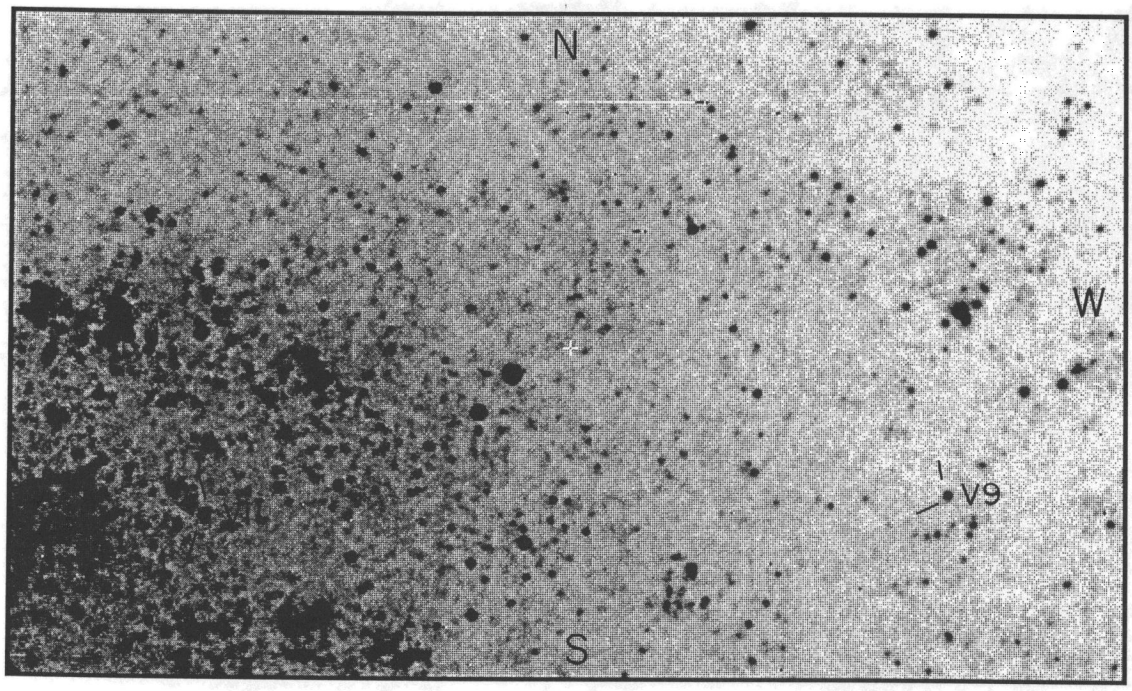

FIG. 2c

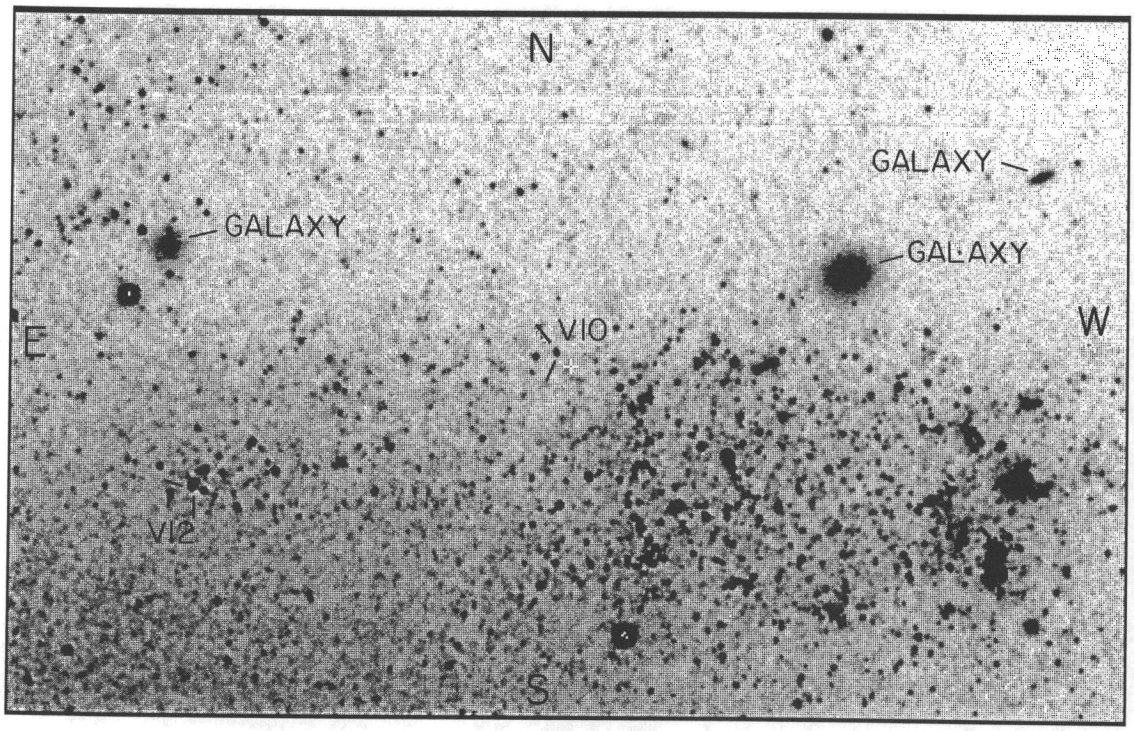

FIG. 2d

to within ± 0.01–0.03 mag of the average for all photometric nights for which an individual filter and field combination was observed. These differences also contain the uncertainty in the aperture corrections applied to determine total magnitudes.

3. CEPHEID MAGNITUDES AND PERIODS

Graham (1984) gives photographic B and V photometry for 18 Cepheids in NGC 300. The time baseline over which he obtained preliminary periods spanned ~ 2000 days. Our CCD data were obtained over a comparable time interval and are separated from the photographic observations by another interval of similar size. In total, the observational baseline on the NGC 300 Cepheids is now ~ 16 years, which, depending on the period of the individual Cepheid, represents a range of ~ 45–650 cycles.

The longer time baseline now available was used to refine

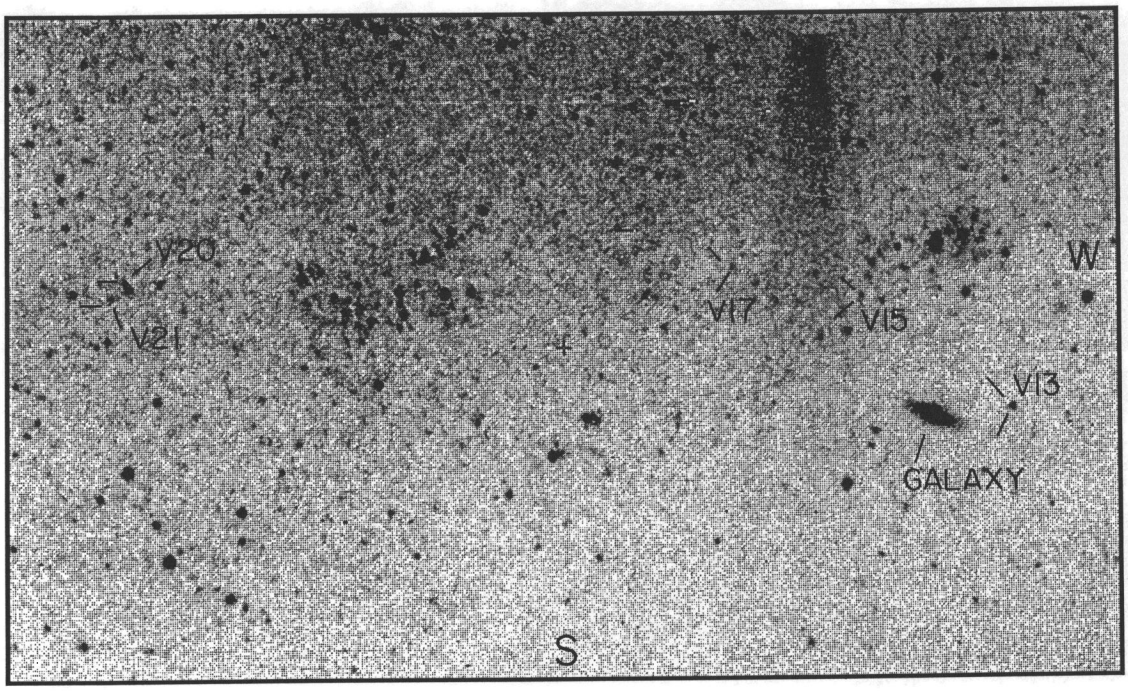

FIG. 2e

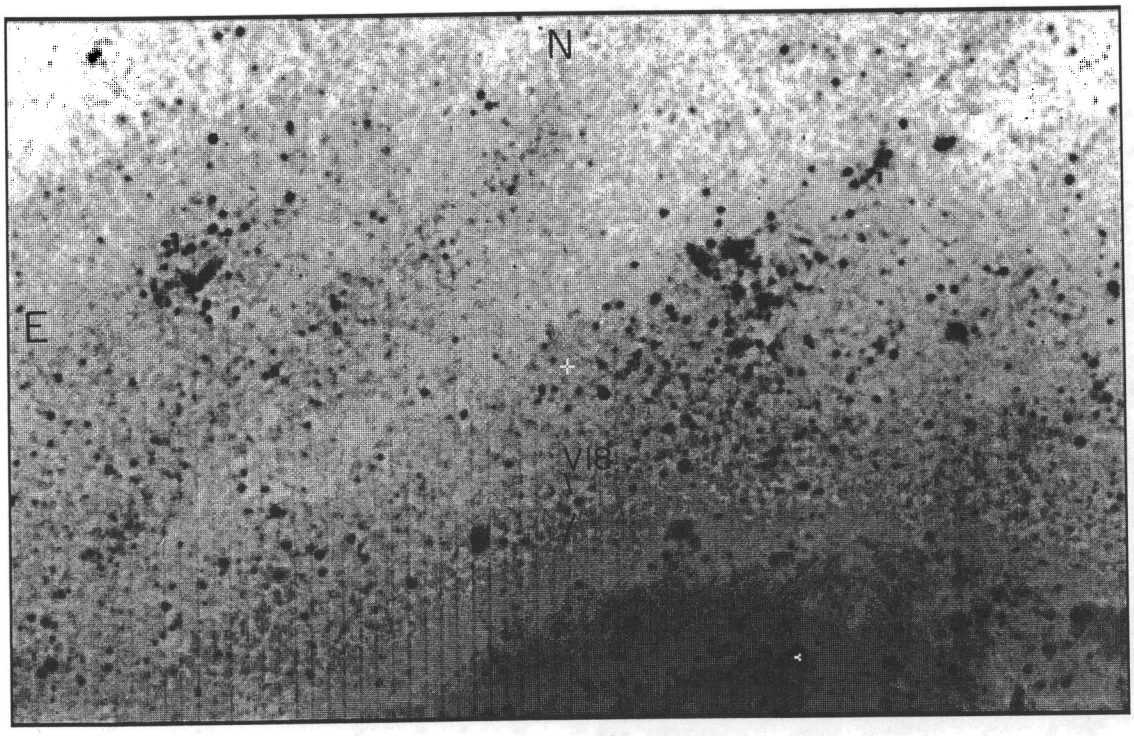

FIG. 2f

the periods of the NGC 300 Cepheids. Before proceeding, however, it was necessary to bring the photographic and CCD data onto the same photometric scale. Walker (1989) recently found a photometric scale and zero point error in Graham's faint photoelectric sequence. Adopting a correction for the photographic data, the periods were refined by demanding phase agreement (in both B and V) between the two sets of observations. The details of the procedure follow below.

Walker's study of the Graham comparison sequence is very sparsely delineated in the magnitude range corresponding to the majority of the Cepheid observations. Furthermore, any magnitude adjustments obtained from his correction curves might not necessarily apply to the Cepheids (which were observed against the background of the galaxy as opposed to the clear sky where the standards were found). Therefore it was decided to use the Cepheid observations themselves to derive

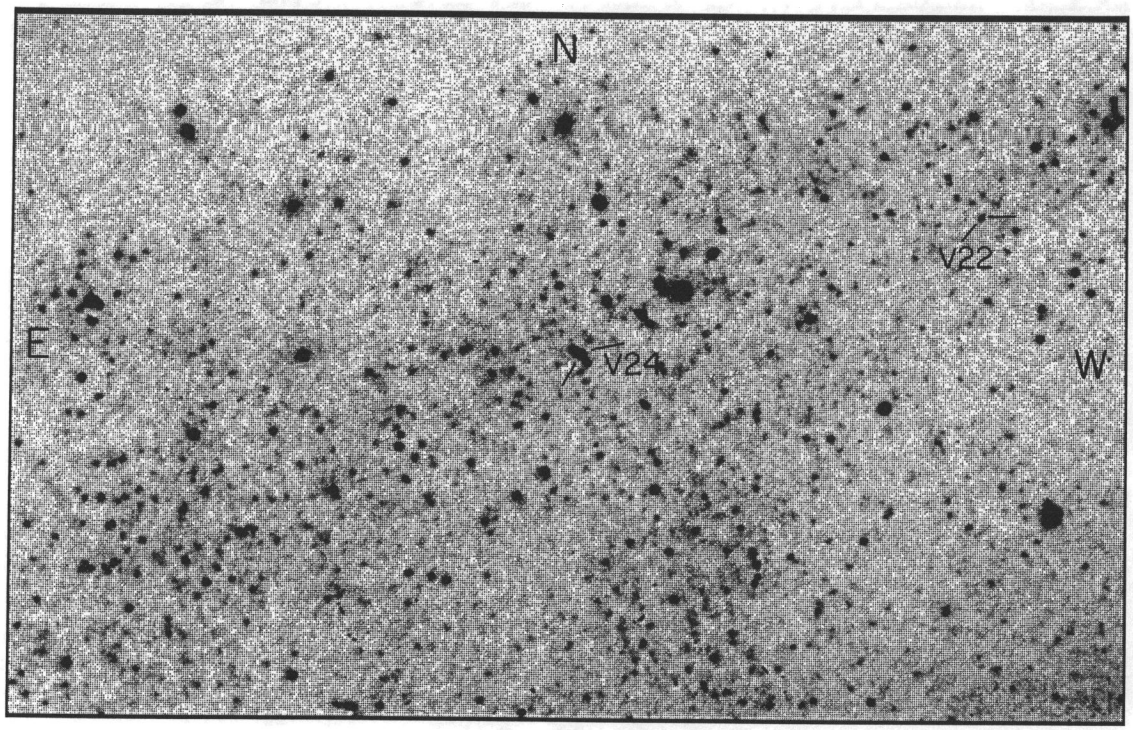

FIG. 2g

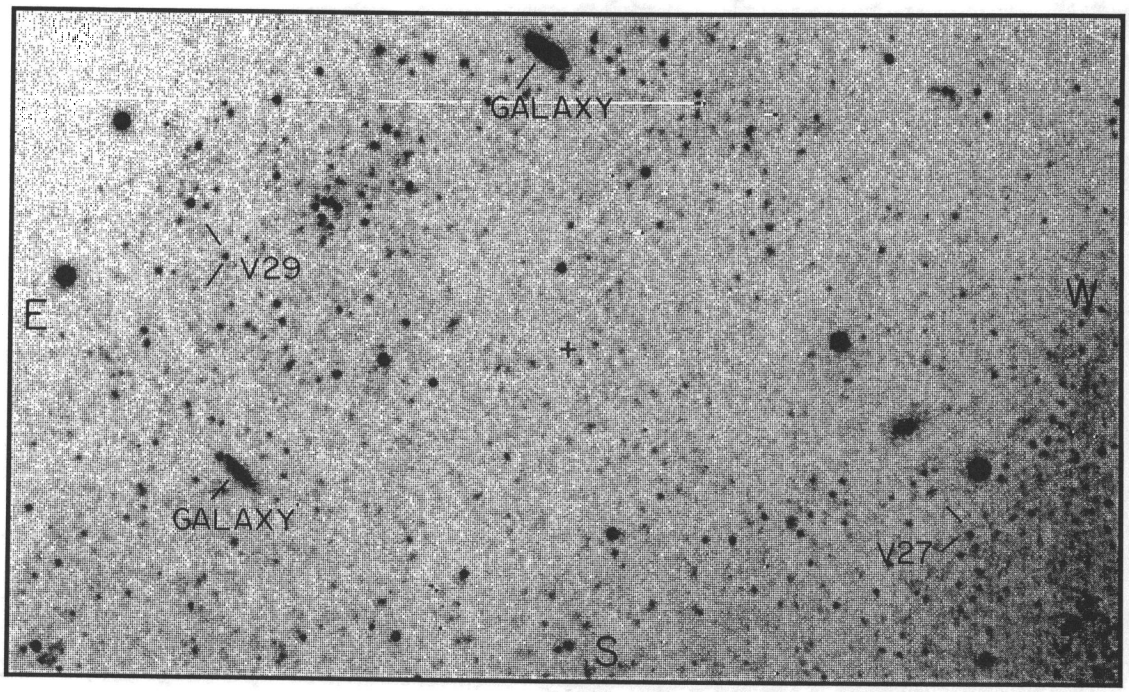

FIG. 2h

the correction formulae to bring the photographic data onto the CCD system.

In principle, one could compare the phased CCD observations individually with the phased photographic data, and thereby derive differential corrections as a function of magnitude throughout the pulsational cycle. This could then be done for each Cepheid, yielding corrections over the entire magnitude range covered by the Cepheid variations. Unfortunately the noise in the photographic data, combined with the obvious phase shifts seen in the two data sets (signaling the need for period adjustments) forced us to adopt a compromise solution, which in the end proved quite satisfactory. In the adopted calibration, we simply compared the mean magnitude of the photographic data with the mean of the CCD data for each Cepheid and plotted these differences as a function of magnitude. In this way, a mean correction formula for the photogra-

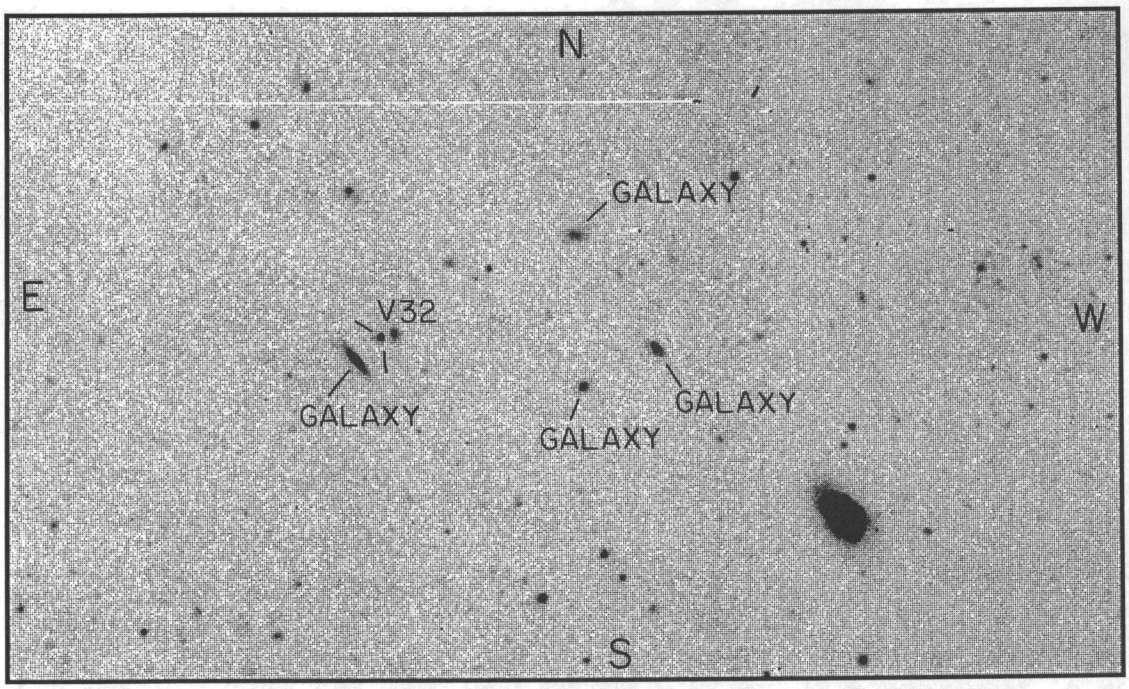

FIG. 2*i*

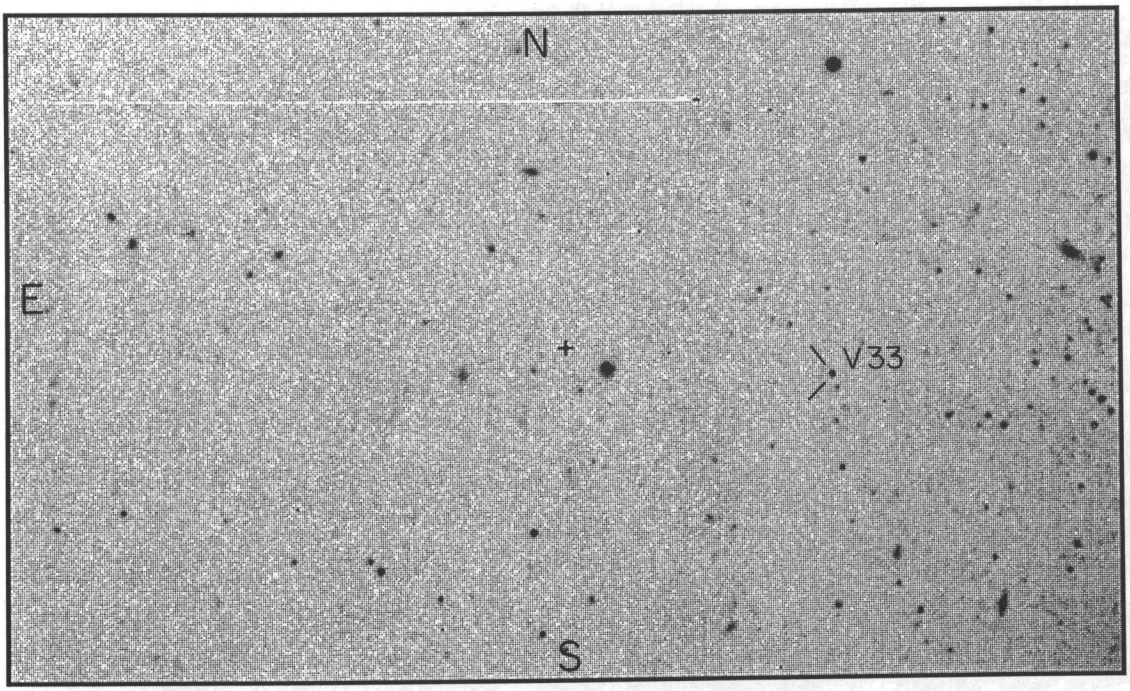

FIG. 2*j*

phic data was generated. In the range covered by the Cepheid observations we derived the following linear interpolation formulae:

$$V_{\rm CCD} = 1.25 \times V_{\rm Graham} - 4.94\ ,$$

$$B_{\rm CCD} = 1.21 \times B_{\rm Graham} - 4.36\ .$$

Note that these relations in fact fall within Walker's (1989) nonlinear error curves quite well. (They refer, however, only to a small, and linear, part of the magnitude range considered by him).

Using the above correction formulae, Graham's photographic Cepheid data were brought onto the CCD system. The two sets of observations (CCD and photographic) were again phased and replotted using Graham's periods and times of maxima. In all but four cases (V2, V18, V22, and V33) noticeable phase shifts were seen between the two data sets, indicating the need to rederive and adjust the periods. This was done

iteratively by (1) measuring the average phase shift between the two B data sets, (2) scaling this mismatch into a period correction using the average number of cycles elapsed between the two data sets, and (3) replotting the data with the new period and making any second-order changes required by an intercomparison of the simultaneous fits in both the B and the V bandpasses. In most cases the method converged in only two iterations, the outstanding exception being V12, which is discussed below. On average, the fractional adjustments to the periods were only a few parts in 1000, largely consistent with the precision quoted for the published periods.

We now discuss some of the individual Cepheids in detail (the revised, adopted periods for all the Cepheids being given in Table 2).

V12.—No satisfactory phase shift could be found to correct the period of the Cepheid and bring the photographic and CCD data into alignment. However, Graham's period of $89^{d}.40$ phases our CCD data extremely well. Thus we have retained Graham's period, and suggest that V12 has undergone a stillstand or comparable phase shift amounting to half a cycle in the last 30.

V13.—The light curve of this variable is very well defined by the CCD data in V, R, and I; however, here are several discrepant phase points in the B light curve. One is at minimum light, the brighter of which has been ignored in drawing the light curve (after consideration of the VRI light curves). Another discrepant point lies on the early part of the descending branch of the light curve. This latter point, combined with the two observations at approximately the same magnitude following it, might have indicated a bump in the descending light curve had it been supported by the other colors. However, in VRI there is only weak evidence for such a feature. We have adopted a revised period of $33^{d}.978$.

V20.—Guided by the photographic data it is apparent that the CCD observations did not define minimum light well; however, maximum light is very well specified, and in fact even minimum light only requires a modest extrapolation. The new period determined here is $18^{d}.007$.

V21.—The exact form of the light curve for this variable is in doubt. The CCD observations completely missed the maximum as defined by the photographic observations. The latter, however, indicate a very flat topped and prolonged maximum, rather uncharacteristic of Cepheids in general. Two solutions have been proposed: in the first, the flat-topped form from the photographic data is adopted, giving a blue amplitude of 1.6 mag, and in the second, the normal fast rise and slower decline is fitted to the CCD data at all wavelengths, with a resulting blue amplitude of 2.4 mag. The adopted period is $9^{d}.667$. The quoted magnitude uses the second solution.

V22.—Only two phase points were observed for this Cepheid, but it was possible to make use of the scaled photographic observations where minimum appears to be well established and maximum light reasonably well known. The I observation at minimum light has been given little weight in order to keep the I amplitude consistent with the known scaling of amplitude with wavelength; that is, the blue amplitude of 1.6 mag predicts an I amplitude of ~ 0.5 mag. The period of $20^{d}.64$ for V22 is unchanged by our new observations.

V24.—Our two CCD observations of the Cepheid fall at almost the same phase (and, as one might hope, at almost the same magnitude). The photographic data thus delineate the light curve completely. Quite by chance both of these observations are very close to mean light (unlike the cases of V32 and V33). We estimate that the period is $126^{d}.04$, shorter than Graham's estimate of $126^{d}.9$.

V27.—Both maximum and minimum light are fairly well estimated by the CCD data alone, as indicated by a comparison with the blue as visual photographic data. Our adopted period is $35^{d}.01$.

V29.—The CCD data appear to define the light curve of this variable quite unambiguously at all wavelengths in good agreement with the blue photographic data. A new period of $24^{d}.445$ is adopted.

V32.—Both of our CCD observations fall at maximum light as indicated by the photographic data. An adjusted period of $52^{d}.762$ appears to phase the two sets of data well.

V33.—While maximum light seems to have been observed quite fortuitously, our one other CCD observation is only slightly later in phase down along the descending branch of the light curve. Here again the photographic data were critical in determining mean light in all wavelengths.

Based on inspection of the individual light curves, 10 Cepheids in the NGC 300 sample appeared to have sufficiently well determined mean magnitudes for further analysis. The procedure adopted here in producing the time-averaged mean magnitudes is the same as that described in detail in Freedman et al. (1991). *Only the CCD data were used in this process*; the photographic data were only used in the period refinement steps discussed above. In Figures 3*a*–3*l* the adopted light curves are shown superposed on the observations. Digitized and converted to intensities, these smooth curves were used to produce the final mean magnitudes.

For a discussion of the error analysis, the interested reader is again referred to the paper on M33 by Freedman et al. (1991). Typically, a repeat of the fitting procedure produced results that agreed to better than ± 0.05 mag, being dependent of course, on the phase coverage of the light curve. The formal error associated with any given light curve can be derived using the following formula from Freedman et al. (1991):

$$\sigma^2_{\text{total}} = [(\Delta m/12)^2 + (\Sigma\sigma_i^2)/N]/(N-1)\,,$$

where Δm is the amplitude of the light variation, the σ_i are the uncertainties for the individual observations of which there are N in number.

TABLE 2

INTENSITY-MEAN MAGNITUDES FOR SELECTED NGC 300 CEPHEIDS

Cepheid	log P	B	V	R	I	Quality
V2.....	1.251	22.14	21.57	21.22	20.87	a, a, a, a
V3.....	1.752	21.12	20.40	20.01	19.62	b, b, b, b
V8.....	1.635	22.00	20.90	20.43	19.84	c, c, c, c
V9.....	1.261	21.99	21.41	20.94	20.73	d, d, d, d
V10.....	1.398	22.05	21.23	20.88	20.60	a, a, a, a
V12.....	1.951	20.80	19.71	19.19	18.76	a, a, a, a
V13.....	1.531	21.46	20.67	20.27	19.89	b, b, b, b
V18.....	1.975	20.99	19.93	19.40	19.04	f, f, f, f
V20.....	1.255	22.13	21.51	21.09	20.64	b, b, b, b
V21.....	0.985	22.16	21.57	21.19	20.81	f, f, f, d
V22.....	1.315	22.43	21.66	21.33	20.92	d, d, d, d
V24.....	2.101	20.89	19.85	19.32	18.87	f, d, d, d
V27.....	1.544	21.77	20.90	20.45	20.08	a, c, b, a
V29.....	1.388	21.89	21.26	20.84	20.45	a, a, a, a
V32.....	1.722	21.25	20.50	20.00	19.70	f, f, f, f
V33.....	1.385	22.15	21.49	20.97	20.47	c, c, c, c

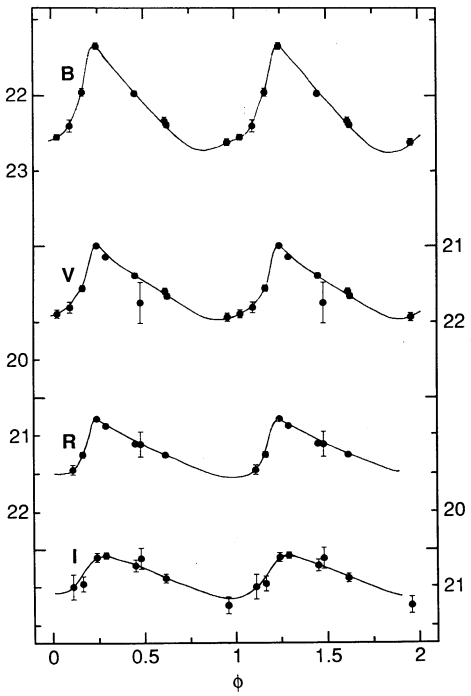

FIG. 3*a*.—V2

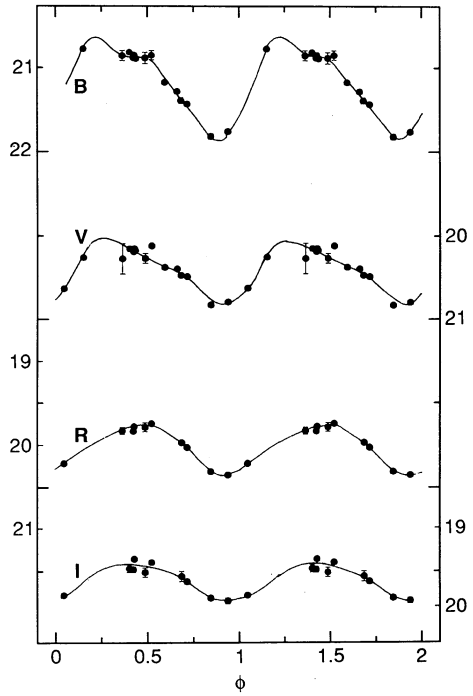

FIG. 3*b*.—V3

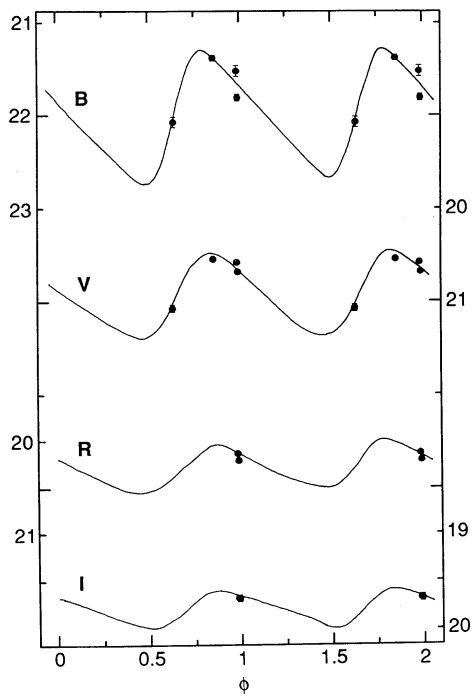

FIG. 3*c*.—V8

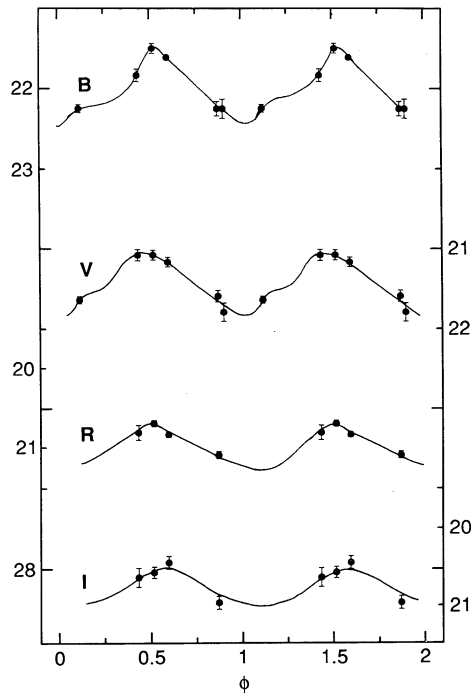

FIG. 3*d*.—V9

FIG. 3.—(*a–l*) *BVRI* light curves for 12 Cepheids observed in NGC 300

4. THE DISTANCE MODULUS OF NGC 300

A number of studies have estimated the distance to NGC 300 independently of the Cepheid distance scale. Among these are the early (and large) estimates of $(m - M)_0 = 27.0$ mag by de Vaucouleurs (1972), and 28.33 mag by Sandage & Tammann (1975). These were followed by Graham (1982) who used photographic magnitudes of what he assumed to be the brightest red giants in NGC 300 to estimate the distance with respect to NGC 205, resulting in a proposed modulus of 25.8 ± 0.5 mag. In a subsequent study, Lawrie & Graham (1983) estimated $(m - M)_0 < 25.90 \pm 0.27$ mag based on the brightest planetary nebula, and $(m - M)_0 = 25.85 \pm 0.34$ mag using the cumulative planetary nebula luminosity function.

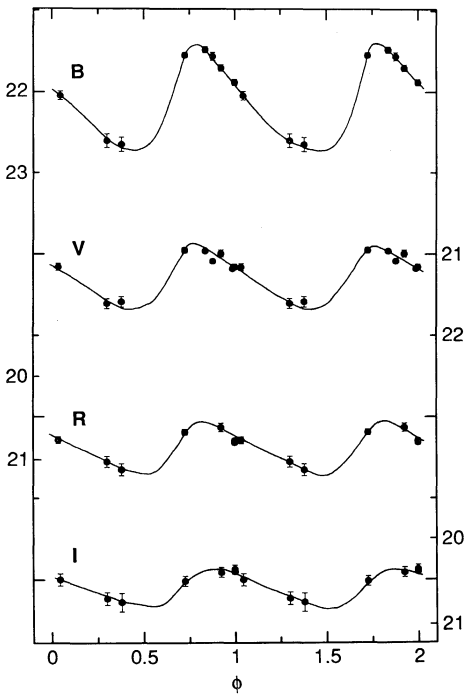

FIG. 3*e*.—V10

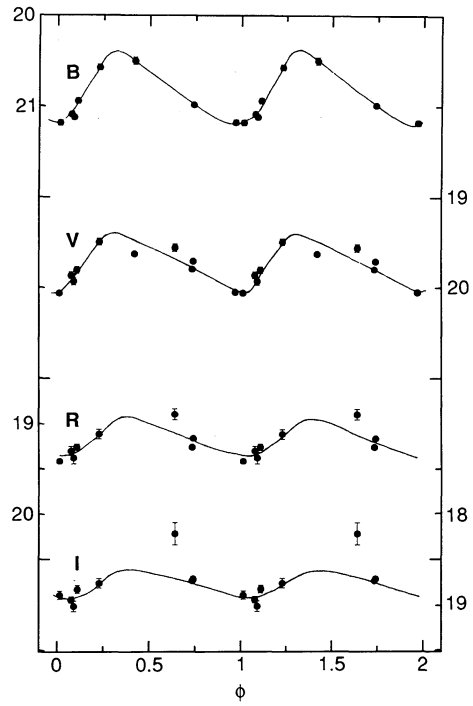

FIG. 3*f*.—V12

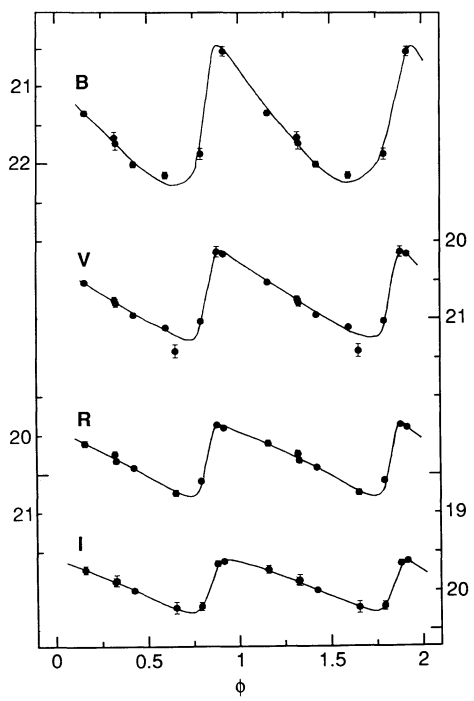

FIG. 3*g*.—V13

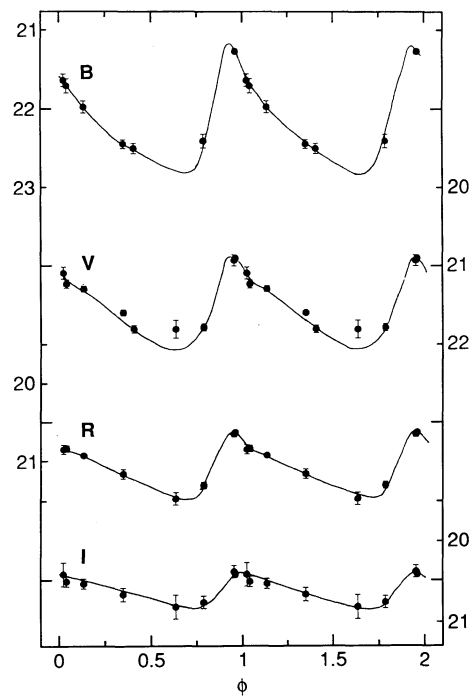

FIG. 3*h*.—V20

More recently Richer, Pritchet, & Crabtree (1985) have presented additional evidence for a low distance modulus (25.92 ± 0.2 mag) using the luminosities of carbon stars in NGC 300 in comparison with similar stars in the LMC [their value adjusted to $(m - M)_0 = 18.5$ mag]. And finally, Carignan (1985) has compiled various determinations following de Vaucouleurs, giving moduli ranging from 26.08 to 26.63 mag, with a global average of 26.39 ± 0.20 mag. This average was then lowered to 26.27 ± 0.20 mag in a subsequent paper (Puche & Carignan 1988) where some of the previously quoted distance determinations were also included.

For the Cepheids alone, the results have remained much the same. Scaling Graham's (1984) Cepheid distance modulus to a common LMC true modulus of 18.5 may yields $(m - M)_0 =$

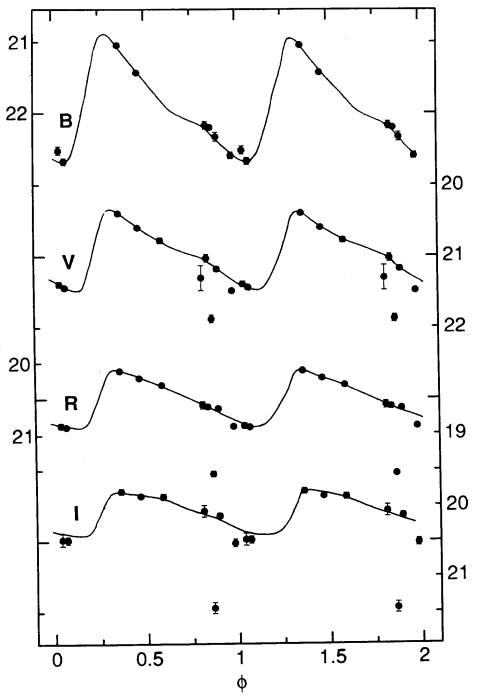

FIG. 3*i*.—V27

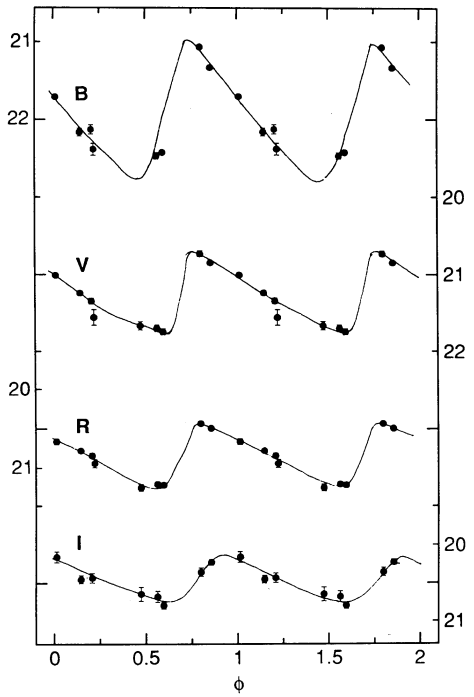

FIG. 3*j*.—V29

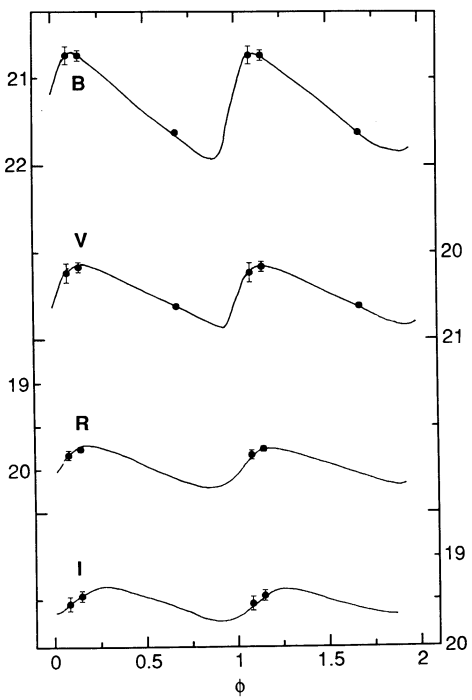

FIG. 3*k*.—V32

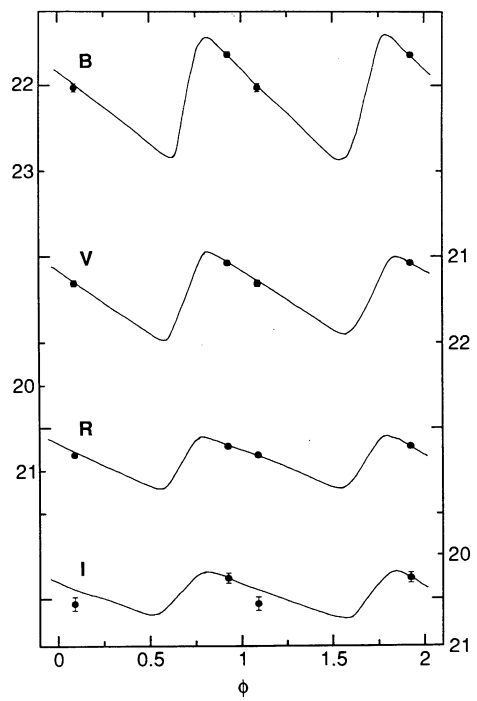

FIG. 3*l*.—V33

26.03 ± 0.20 mag, while Madore et al. (1987) give $(m - M)_0 = 26.30 \pm 0.25$ mag based on their interpretation of *H*-band photometry. Finally, Walker's (1988) reassessment of the Graham photographic data gives $(m - M)_0 = 26.4 \pm 0.2$ mag. To within 10%, the Cepheid studies yield agreement that the distance to NGC 300 is 2 Mpc. We now discuss the new multiwavelength *BVRI* PL relations.

4.1. *Period-Luminosity Relations*

In keeping with the previous papers of this series, we make all comparisons of the PL relation for the Cepheids in NGC 300 with the corresponding photoelectric data for Cepheids in the Large Magellanic Cloud, as compiled by Madore (1985). This allows for a consistent set of distant moduli to be present-

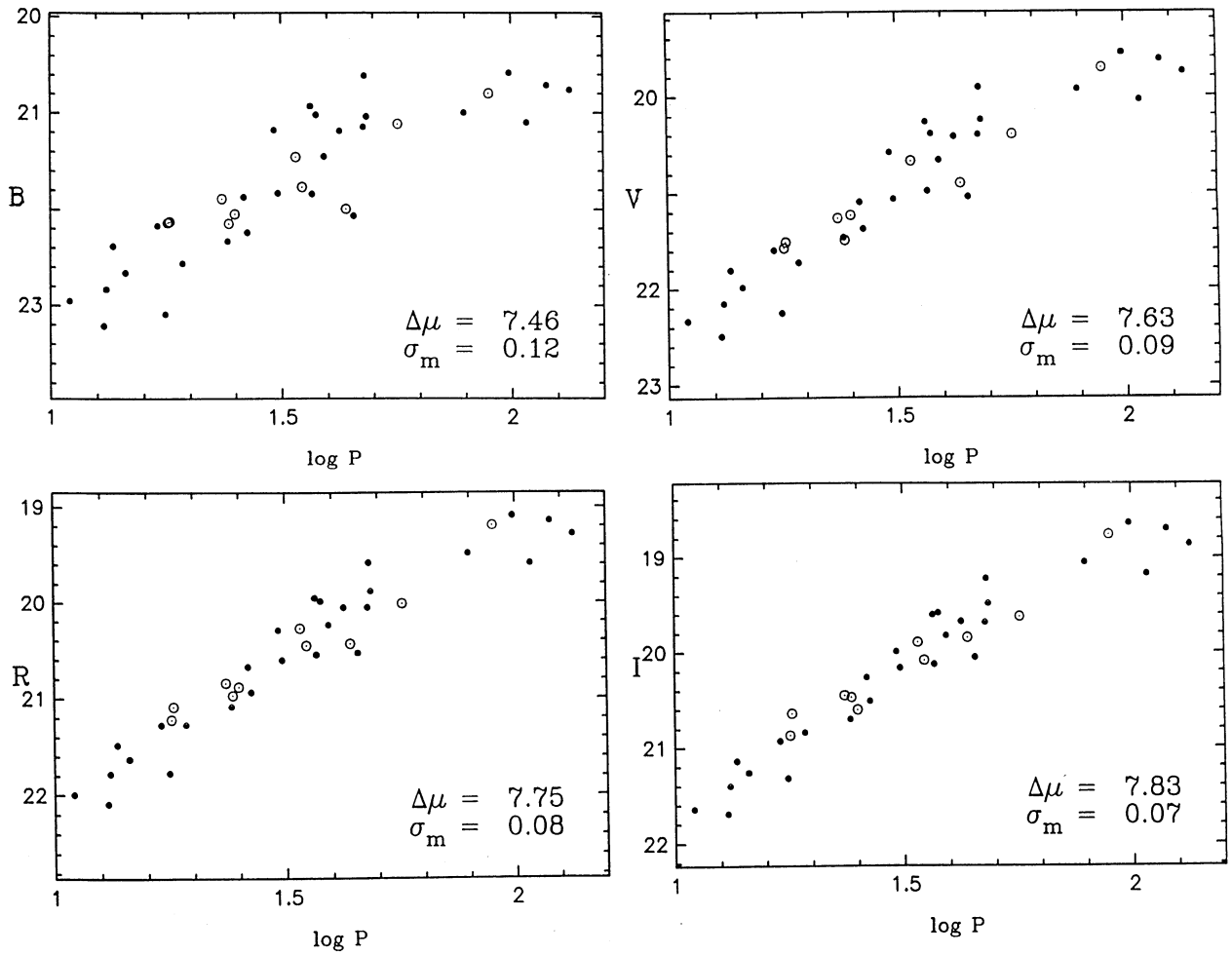

FIG. 4.—The time-averaged *BVRI* period-luminosity relations for the Cepheids in NGC 300. Open circles mark the best NGC 300 CCD data (as discussed in text) and filled circles denote the time-averaged photoelectric data given in Madore (1985) and Walker (1987) for the Large Magellanic Cloud Cepheids.

ed from paper to paper and also provides for a simple translation of all the previous solutions should a different combination of true distance modulus and foreground reddening for the LMC be preferred. Or, as discussed below, simple offsets can be applied in the event that there is a demonstrated need, say, for an additional reddening term internal to the LMC.

The intensity-mean *BVRI* $P - L$ relations for our 10 best-observed Cepheids in NGC 300 (V2, V3, V8, V10, V12, V13, V20, V27, V29, and V33, as individually discussed above, and having light curve qualities "*a*" [excellent], "*b*" [good], or "*c*" [fair], as listed in Table 2) are shown in Figure 4. As expected, the dispersion of points in any given bandpass is significantly reduced in comparison to the corresponding random-phase data plot shown in Figure 5. More importantly, the final dispersion is very similar to the dispersion seen in the time-averaged LMC sample, a result also seen for the Cepheids in M33 (Freedman et al. 1991) and in IC 1613 (Freedman 1988a).

4.2. *Reddening*

With the various multicolor apparent moduli (relative to the LMC sample), is is possible to derive an estimate of the total reddening to the target galaxy, assuming that all of the wavelength dependence is due to extinction. To do this we must first assume that the reddening law appropriate to NGC 300 is the same as that in the Galaxy. For this series of papers we have adopted the relations derived by Cardelli, Clayton, & Mathis (1989). The ratio of total-to-selective absorption is taken to be $R_V = 3.3$, a value appropriate for late-type stars like Cepheids. Furthermore, all that is directly derived by us is a differential reddening above or below that of the total reddening to the LMC Cepheids. Currently we are adopting a total line of sight reddening for the LMC Cepheids of $E(B-V) = 0.10$ mag. This latter correction has then been appropriately scaled to each of the observed wavelengths, and added to each of the relative apparent moduli derived from the comparison of the galaxy data and the LMC apparent data. Finally, to set the absolute zero point we adopt a true modulus of $(m - M) = 18.5$ mag for the LMC. The individual absolute distance moduli for each wavelength as corrected for the adopted LMC reddening and distance modulus are given in Table 3.

The moduli resulting from the above procedure are shown plotted as a function of inverse wavelength in Figure 6. The dashed line is the χ^2 minimized fit of the adopted interstellar extinction law to the moduli. The intercept of this nonlinear function at $1/\lambda = 0$ corresponds to a true distance modulus for NGC 300 of $(m - M)_0 = 26.66 \pm 0.10$ mag.

Note that what we actually measure is the total reddening *difference* between NGC 300 and the LMC Cepheid sample.

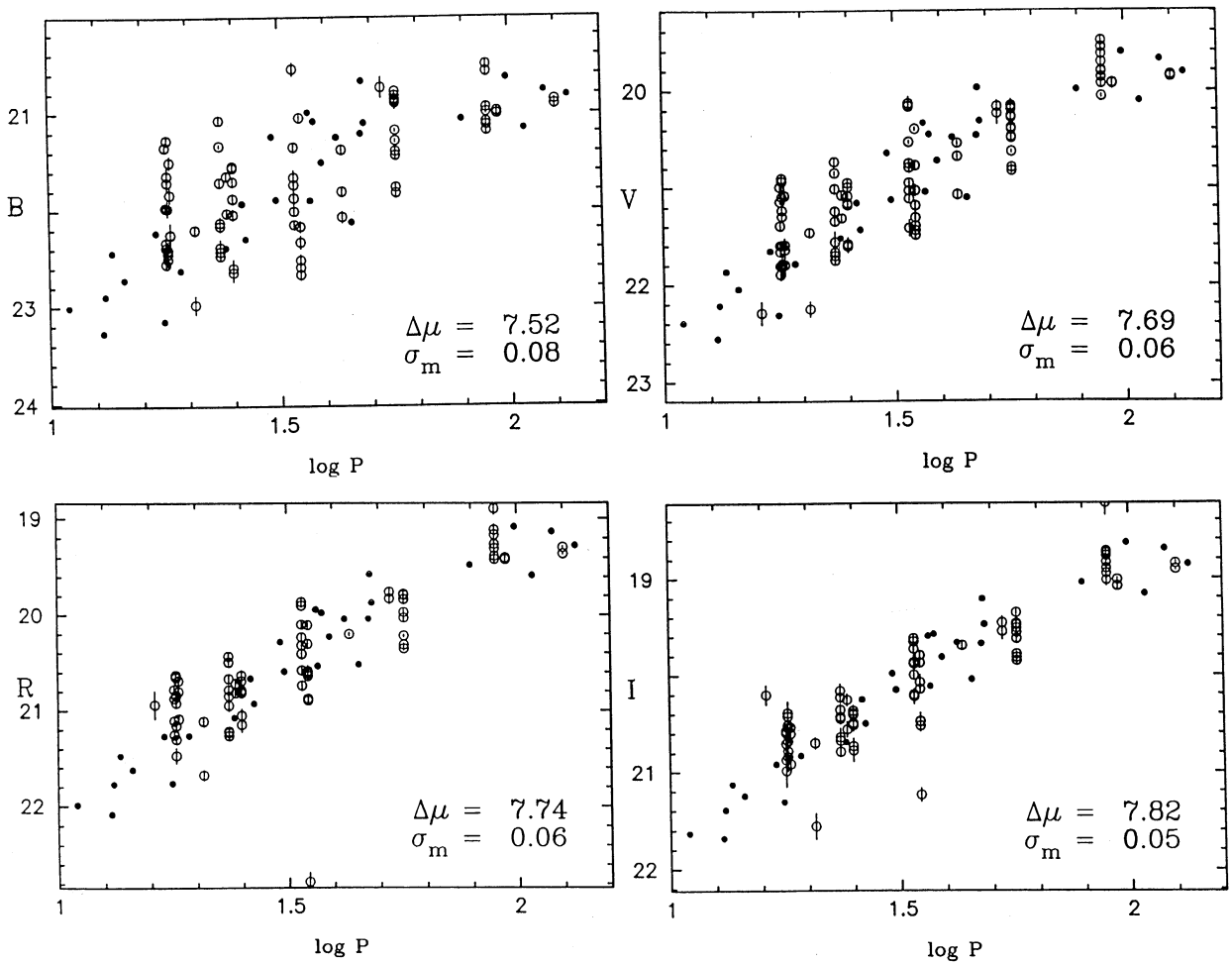

FIG. 5.—The same as Fig. 4 except that the open circles are now all of the individual CCD observations for the NGC 300 Cepheids uncorrected for phase

In this case it is $E(B-V)_{N300} - E(B-V)_{LMC} = -0.17$ mag. The time-averaged data set, adopting $E(B-V)_{LMC} = 0.10$ mag, gives for NGC 300 a total reddening of $E(B-V) = -0.07 \pm 0.03$ mag; the random-phase data solution gives $E(B-V) = -0.03$ mag. Both of these reddenings are negative. We now discuss the derivation of these specific values, and the implications in some detail. A negative value for reddening makes no physical sense, in terms of what we know about the interstellar medium. However, a negative *formal* solution could be an important result, because it might for instance imply that the intrinsic colors of the NGC 300 Cepheids are systematically and intrinsically bluer than those in the fiducial (LMC) sample, thereby leading to an underestimation of their reddening. The obvious alternative point of

TABLE 3

NGC 300 CEPHEID MULTIWAVELENGTH APPARENT AND TRUE DISTANCE MODULI[a]

Filter	Time-Averaged Modulus	Random-Phase Modulus
B	26.37	26.42
V	26.45	26.50
R	26.49	26.48
I	26.52	26.51
μ_0	26.66	26.58
$E(B-V)$	−0.07	−0.03

[a] $E(B-V)_{LMC} = 0.10$ and $(m-M)_0 = 18.5$ mag.

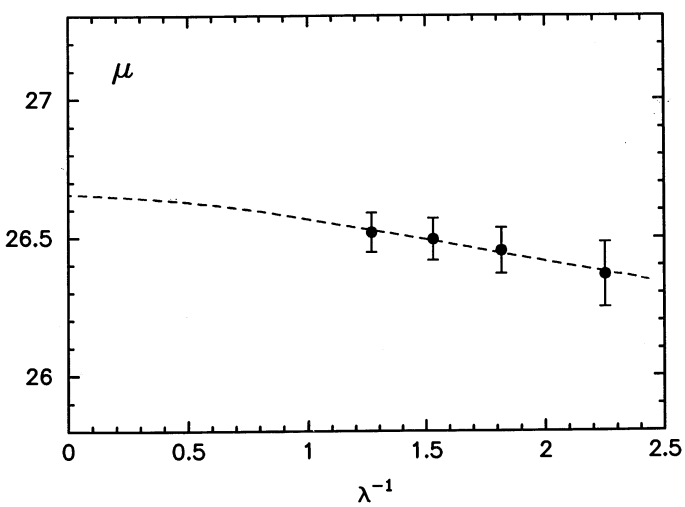

FIG. 6.—The NGC 300 apparent distance moduli obtained for each wavelength band as derived from time-averaged Cepheid light curves, plotted as a function of inverse wavelength (in μm^{-1}). A chi-squared fit to the data yields an intercept or true relative distance modulus of 26.66 ± 0.10 mag.

view is that the LMC Cepheids are too red, in the sense that they have not been sufficiently corrected for their own reddening.

For the NGC 300 sample, the derived reddening becomes nonnegative if the total (foreground and internal) reddening to the LMC Cepheid sample is $E(B-V) = 0.17$ mag. However, this solution still leaves both the foreground Galactic reddening to NGC 300 *and* the internal reddening to NGC 300 itself identically equal to zero. Since NGC 300 is a fairly gas rich Sc galaxy, unless it has an extremely low dust-to-gas ratio, it seems unlikely that all of the NGC 300 Cepheids in our sample have lines of sight that intersect no dust. Note, however, that published *foreground* reddening estimates in the direction of NGC 300 are low [for instance, Burstein & Heiles (1984) estimate a Galactic foreground reddening of $E(B-V) = 0.025 \pm 0.02$ mag, which is consistent with zero.] Furthermore, NGC 300 also appears to be generally dust-free as indicated by (*a*) The color of its resolved young stellar population is extremely blue ($\langle B-V\rangle_{MS} \simeq -0.25$ mag; Pierre & Azzopardi 1988). (*b*) Its over-all integrated colors are comparably blue or bluer than the other two late-type galaxies in the Sculptor Group (NGC 247 and NGC 7793) for which $(U-J)$ and $J-F$) surface photometry is also available. (In addition, see the strikingly blue, color photograph of NGC 300 in Lausten, Madsen, & West 1987). (*c*) An inspection of our CCD frames reproduced in Figures 2*a*–2*i* shows that there are numerous (background) galaxies visible through the (generally outer) regions of NGC 300 in which the known Cepheids are located, indicating that there are at least some regions of low total line-of-sight extinction. Unfortunately, all of these arguments are circumstantial, and at the present time the best that can be said is that the total reddening to the NGC 300 Cepheids is low, and probably less than or of order $E(B-V) = 0.1$ mag.

Before leaving this discussion, we note that a larger value for the LMC Cepheid reddenings may be indicated by a study of a subset of Cepheids in M31, specifically those Cepheids in Baade's 20 kpc outer Field IV. In that case the reddening derived for the M31 Cepheids is nonnegative (Freedman & Madore 1990), but is is smaller than that predicted for the foreground Galactic component alone. To have the M31 Cepheid data minimally consistent with the H I reddenings of Burstein & Heiles (1984) also requires the total LMC reddening to be $E(B-V) = 0.17$ mag. In that case again, the formal solution still allows for no reddening internal to the field in M31 itself.

It is beyond the scope of this paper to adequately assess the absolute reddening appropriate to the individual (or mean sample of) LMC Cepheids (but see Bessell 1991). However, we note that adopting a larger value is not inconsistent with reddening determinations for other LMC supergiants (Grieve & Madore 1986). Furthermore such a value would only require the addition of an internal LMC reddening component that is comparable to the often-quoted foreground Galactic reddening in the direction of the LMC of $E(B-V) = 0.08$ mag. Nevertheless, we stress here that we do not derive absolute reddenings for the NGC 300 Cepheids or any of the Cepheids discussed in this series of papers. We only measure a difference in apparent moduli, from which we derive a *difference in reddening*. Absolute calibration, and the evaluation of components ascribable to the Galactic foreground or to the parent galaxy require additional assumptions and/or independent data. But, our derivation of a true distance modulus using the multiwavelength fitting procedure is in fact independent of any *absolute* determination of the reddening, and depends only on the adoption of a true distance modulus to the LMC and the assumption that reddening is responsible for the differences in the apparent moduli.

4.3. *The VI Solution*

Since *Space Telescope* will be using only V and I filters for its determination of the reddening and distance moduli to its sample of Cepheids in nearby galaxies, it is of interest to ask how well these two filters reproduce the more extensive multiwavelength solutions. The results are very encouraging. Using only the V and I data for NGC 300 gives $(m-M)_0 = 26.62$ mag and $E(B-V) = -0.05$ mag; and these values are not significantly different from the values quoted above (see Table 3).

4.4. *Reddening-free PL Relations*

Finally, we present the solution for the NGC 300 distance modulus using the reddening-free function $W = V - R_V \times (B-V)$, where R_V is the ratio of total-to-selective absorption taken to be 3.3. Figure 7 shows the comparison of the NGC 300 data with the LMC W-log P plot, from which we derive a true modulus of $(m-M)_0 = 26.76 \pm 0.10$. The difference between this solution and the full multiwavelength solution is likely due to several differences in the methods used: (1) the W solution has the advantage that it implicity corrects not only the NGC 300 data for all reddening (foreground and internal), but it also corrects the LMC data without any need for assumptions about the amount of reddening to or within either system. (2) The disadvantage of the W solution is that it depends entirely upon only two of the four available colors, making it statistically less accurate. (3) Finally, W is dependent upon the *least secure* of the available magnitudes, B and V, which because of their large amplitudes are hardest to define with a finite sampling of the light curve. Given the above comments, we defer placing any undue significance on the difference between the W solution and the multiwavelength modulus. We note, however, that Table 3 and Figure 6 show that a reddening-curve fit through the B and V data alone would also result in a

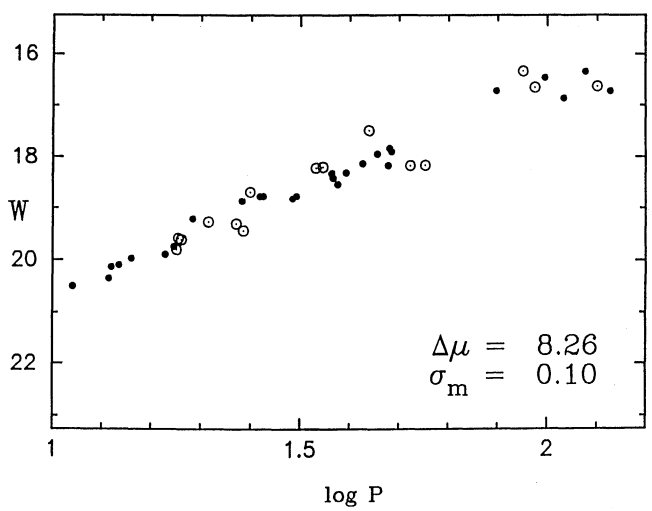

FIG. 7.—The reddening-free W-log P relation for the NGC 300 Cepheids (*open circles*), compared to the LMC Cepheids (*filled circles*) corresponding to a true distance modulus of 26.76 ± 0.10 mag for NGC 300.

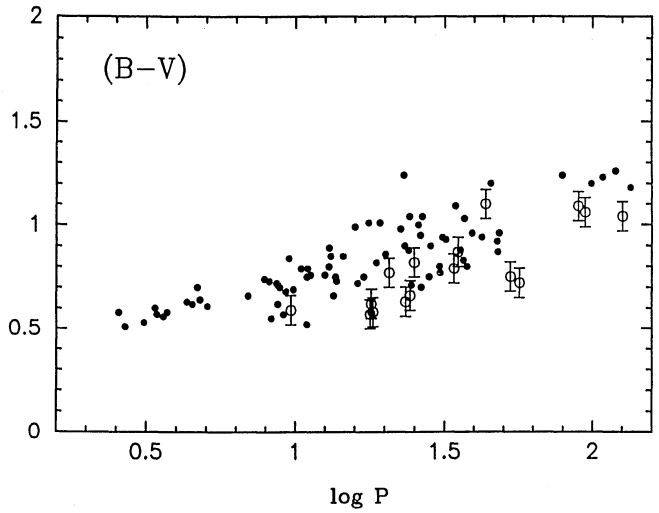

FIG. 8.—Period-$(B-V)$ color relation for the NGC 300 Cepheids (*open circles*), compared to the LMC Cepheids (*filled circles*). No corrections for reddening have been applied to either data set.

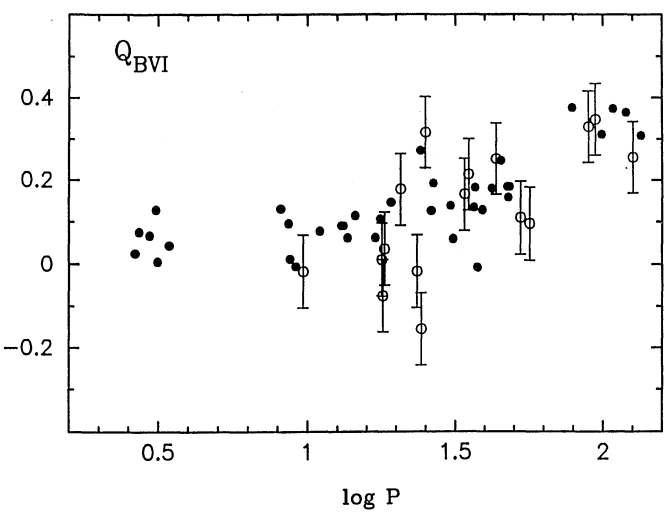

FIG. 9.—The reddening-free color Q-log P relation for the NGC 300 Cepheids (*open circles*), compared to the LMC Cepheids (*filled circles*).

larger true distance modulus, and would again suggest more reddening for the LMC sample [$\Delta E(B-V) = +0.08$ mag if the time-averaged data are considered, or $\Delta E(B-V) = +0.07$ mag if the random-phase data are used.]

5. THE PERIOD-COLOR RELATION

A period-color, $(B-V)$ versus log P, relation for the Cepheids in NGC 300, compared to those in the LMC, is illustrated in Figure 8. The NGC 300 Cepheids are plotted as open circles, and the LMC data are again plotted as solid symbols. In this figure no correction for any reddening has been applied to either the NGC 300 or the LMC data set. The slopes and the widths of the two period-color distributions show no significant differences, however, the LMC Cepheids appear on average to be somewhat redder (by ~ 0.2 mag) at any given period when compared to the NGC 300 sample.

The *apparent* difference in mean color seen here could be due to intrinsic differences in the two samples; it could be entirely due to a difference in mean reddening, or of course, it could be due to a combination of both of these effects. To attempt to resolve this ambiguity, a reddening-free $Q(BVI)$ versus log P plot for the NGC 300 and LMC Cepheids is shown in Figure 9, again with open (NGC 300) and closed circles (LMC), respectively. Q is defined to be reddening-free by having $Q = (B-V) - X(V-I)$ where $X = E(V-I)/E(B-V) = 0.80$. In this representation, the widths and slopes of the two distributions are the same, and the means for the two distributions as a function of period are very similar. The scatter for the NGC 300 data is larger, but it is consistent with the random photometric errors in the NGC 300 colors. The similarity in the mean of the two distributions in this reddening-free representation suggests that the colors of the Cepheids in the two systems are not intrinsically different, and that the apparently bluer $(B-V)$ colors of the NGC 300 Cepheids at a given period are again due to the larger total reddening of the LMC sample relative to the NGC 300 sample.

The staff at CTIO and the various members of the TAC are thanked for their generous support of this program over the many years it took to accumulate the necessary data in the service observing mode. BFM was supported in part by the Jet Propulsion Laboratory, California Institute of Technology, under the sponsorship of the Astrophysics Division of NASA's Office of Space Science and Applications. Research by W. L. F. into the extragalactic distance scale is supported in part by NSF Grant AST 87-13889.

REFERENCES

Bessell, M. S. 1991, A&A, 242, L17
Burstein, D., & Heiles, C. 1984, ApJS, 54, 33
Cardelli, J. A., Clayton, G. C., & Mathis, J. S. 1989, ApJ, 345, 245
Carignan, C. 1985, ApJS, 58, 107
de Vaucouleurs, G. 1972, ApJ, 224, 710
Freedman, W. L. 1988a, ApJ, 326, 691
———. 1988b, AJ, 96, 1248
———. 1990, ApJ, 355, L35
Freedman, W. L., & Madore, B. F. 1988, ApJ, 332, L63
———. 1990, ApJ, 365, 186
Freedman, W. L., Wilson, C. D., & Madore, B. F. 1991, ApJ, 372, 455
Graham, J. A. 1982, ApJ, 252, 474
———. 1984, AJ, 89, 1332
Grieve, G. R., & Madore, B. F. 1986, ApJS, 62, 427
Landolt, A. 1983, AJ, 88, 439
Lausten, S., Madsen, C., & West, R. M. 1987, Exploring the Southern Sky (Berlin: Springer), 68
Lawrie, D. G., & Graham, J. A. 1984, BAAS, 15, 907
Madore, B. F. 1985, in IAU Colloq. 82, Cepheids: Theory and Observations, ed. B. F. Madore (Cambridge Univ. Press), 166
Madore, B. F., Welch, D. L., McAlary, C. W., & McLaren, R. A. 1987, ApJ, 320, 26
Mateo, M., & Schechter, P. L. 1989, in Proc. ESO Conf. Workshop 31, 1st ESO/ST-ECF Data Analysis Workshop, ed. P. J. Grosbol, F. Murtagh, & R. H. Warmels, (Garching: ESO), 69
Pierre, M., & Azzopardi, M. 1988, A&A, 189, 27
Puche, D., & Carignan, C. 1988, AJ, 95, 1025
Richer, H. B., Pritchet, C. J., & Crabtree, D. R. 1985, ApJ, 298, 240
Sandage, A. R., & Bedke J. 1988, Atlas of Galaxies Useful for Measuring the Cosmological Distance Scale, NASA SP-496 (Washington, DC: NASA)
Sandage, A. R., & Tammann, G. A. 1975, ApJ, 196, 313
Walker, A. R. 1988, PASP, 100, 949